Dual-emitting Mn(II) and Zn(II) halide complexes with 9,10-dihydro-9-oxa-10-phosphaphenanthrene-10-oxide as ligand

Valentina Ferraro [a], Jesús Castro [b], Lodovico Agostinis [c], Marco Bortoluzzi [a,d,*]

[a] Dipartimento di Scienze Molecolari e Nanosistemi, Università Ca' Foscari Venezia, 30172 Mestre VE, Italy
[b] Departamento de Química Inorgánica, Universidade de Vigo, Facultade de Química, Edificio de Ciencias Experimentais, 36310 Vigo Galicia, Spain
[c] Aimplas, Plastic Technology Center, Valencia Parc Tecnologic, C/Gustave Eiffel, 4, 46011 Valencia, Spain
[d] Consorzio Interuniversitario Reattività Chimica e Catalisi (CIRCC), via Celso Ulpiani 27, 70126 Bari, Italy

ARTICLE INFO

Keywords:
Manganese
Zinc
Tetrahedral complexes
Photoluminescence
H-phosphinate

ABSTRACT

The *H*-phosphinate 9,10-dihydro-9-oxa-10-phosphaphenanthrene-10-oxide (DOPO) acts as O-donor ligand towards manganese(II) and zinc(II) halides, with the formation of tetrahedral complexes having general formula $[MX_2(DOPO)_2]$ (M = Mn, X = Cl, Br, I; M = Zn, X = Br). The structure of $[ZnBr_2(DOPO)_2]$ was ascertained by single-crystal X-ray diffraction. All the compounds showed appreciable photoluminescence at the solid state, with an emission band in the red region of the spectrum attributed to radiative decay from triplet states of the coordinated DOPO ligands. Such an emission is superimposed to the $^4T_1(^4G)\rightarrow{}^6A_1(^6S)$ transition around 530–540 nm in the case of the Mn(II) derivatives and to a fluorescent band centred at 380 nm for $[ZnBr_2(DOPO)_2]$. Excitation wavelength-dependent emission was observed for $[MnCl_2(DOPO)_2]$ and $[MnBr_2(DOPO)_2]$. The absorption and emission features of the coordinated DOPO ligands were rationalized by means of TD-DFT calculations.

1. Introduction

Phosphine oxides are widely investigated for their photophysical properties, deeply influenced by the electronic and steric features of the phosphorus-bonded substituents [1–4]. Organic compounds containing the {O=P} fragment can exhibit both fluorescence and phosphorescence, depending upon the nature of the substituents. The emission, often centred in the violet-blue region of the visible spectrum, is of current interest for advanced technology. In particular, highly efficient materials characterized by blue phosphorescence or thermally activated delayed fluorescence (TADF) are promising to be applied in organic light emitting diodes (OLEDs) [5–17].

In the perspective of sustainability, the application of pure organic or earth-abundant derivatives to be exploited for optoelectronic is highly desirable [18–21]. Oxygen-donor ligands based on pentavalent phosphorus proved to be a viable choice to isolate Mn(II) complexes characterized by emissions related to the $^4T_1(^4G)\rightarrow{}^6A_1(^6S)$ transition and centred between the green and the red regions of the spectra depending upon the coordination geometry [22–26]. Mono- and polydentate phosphines, phosphoramides, amidophosphates and phosphonates resulted suitable for the preparation of luminescent Mn(II) compounds, sometimes behaving as multifunctional materials [27–40]. Another sustainable metal centre for OLED technology is zinc [41]. Zn(II) compounds with [O=P]-donor ligands were much less investigated, not only for what concerns their photophysical features, but also under a structural point of view. Non-linear optical properties were however observed for $[ZnCl_2(O{=}PPh_3)_2]$ [42], and Zn(II) halide complexes with *N*,*N*,*N*',*N*'-tetramethyl-*P*-indol-1-ylphosphonic diamide showed intense green phosphorescence [43]. An intriguing feature recently emerged for selected first-row transition metal complexes is dual emission, exhibited in particular by Mn(II) derivatives with suitable phosphines and arylphosphonic diamides in the coordination sphere [44–47].

The compounds containing the O=P double bond investigated as luminescent species or as ligands for luminescent complexes are generally based on pentavalent phosphorus. Much less attention was devoted to species containing the {O=P} moiety with phosphorous in lower formal oxidation state, such as *H*-phosphinates. An example of commercially available compound belonging to this class is 9,10-dihydro-9-oxa-10-phosphaphenanthrene-10-oxide (DOPO), commonly used as halogen-free flame retardant [48–55]. The presence of an extended π-conjugated system in a rigid structure and of an oxygen atom potentially suitable for coordination prompted us to study the reaction of

* Corresponding author.
E-mail address: markos@unive.it (M. Bortoluzzi).

DOPO towards Mn(II) and Zn(II) halides and to investigate the luminescence features of the corresponding coordination compounds. In the present paper dual-emitting halide complexes having general formula $[MX_2(DOPO)_2]$ (M = Mn, X = Cl, Br, I; M = Zn, X = Br) are described.

2. Experimental part

2.1. Materials and methods

Commercial solvents (Merck) were purified as described in the literature [56]. Anhydrous MnX_2 halides (X = Cl, Br, I) were purchased from Alfa Aesar, whereas anhydrous $ZnBr_2$ was a Merck product. 9,10-dihydro-9-oxa-10-phosphaphenanthrene-10-oxide (DOPO) was purchased from Fluorochem. The syntheses of all the complexes were carried out under inert atmosphere, working in a glove box (MBraun Labstar with MB 10 G gas purifier) filled with N_2 and equipped for organic and inorganic syntheses. Elemental analyses (C, H, N) were carried out using an Elementar Unicube microanalyzer. Halide content was determined using the Mohr's method [57]. Magnetic susceptibilities were measured on solid samples at 298 K using an MK1 magnetic susceptibility balance (Sherwood Scientific ltd, magnetic field strength 3.5 kGauss) and corrected for diamagnetic contribution by means of tabulated Pascal's constants [58]. Melting points were registered using a FALC 360 D instrument equipped with a camera. Thermogravimetric analyses (TGA) were carried under N_2 atmosphere with a Perkin Elmer TGA 4000 instrument. The heating rate was set at 10 °C min^{-1} from 35 °C up to 500 °C.

IR spectra were collected in the 4000–400 cm^{-1} range using a Perkin-Elmer Spectrum One spectrophotometer. Mono- and bidimensional nuclear magnetic resonance (NMR) spectra were collected employing Bruker Avance 300 and Avance 400 instruments operating respectively at 300.13 MHz and 400.13 MHz of ^1H resonance. ^1H NMR spectra are referred to the partially non-deuterated fraction of the solvent, itself referred to tetramethylsilane. $^{31}P\{^1H\}$ NMR resonances are referred to 85% H_3PO_4 in water. Absorption spectra in dichloromethane or ethanol were recorded with a Yoke 6000Plus double-beam spectrophotometer. Photoluminescence emission (PL) and excitation (PLE) spectra as well as lifetime decay curves were registered on solid samples at room temperature using a Horiba Jobin Yvon Fluorolog-3 spectrofluorometer. Air-tight quartz sample holders were used and filled in the glove box to avoid interactions of the air-sensible complexes with moisture. A continuous wave xenon arc lamp was used as source and the excitation wavelength was selected using a double Czerny–Turner monochromator. Suitable long pass filters were placed in front of the acquisition systems. The detector was composed of a single monochromator iHR320 and a photomultiplier tube Hamamatsu R928. Excitation and emission spectra were corrected for the instrumental functions. Time-resolved analyses were performed in Multi Channel Scaling mode (MCS) or time correlated single photon counting mode (TCSPC) employing Horiba SpectraLED and NanoLED pulsed sources. The room-temperature photoluminescence quantum yields (Φ) at the solid state were measured by means of an OceanOptics HR4000CG UV–vis-NIR detector, fiber-coupled to an integrating sphere connected to OceanOptics UV LED continuous sources ($\lambda_{excitation}^{max}$ = 310 and 365 nm). Values are reported as average of three measurements.

2.2. Synthesis of the complexes

The complexes were prepared by slowly adding a solution containing 2.1 mmol (0.455 g) of 9,10-dihydro-9-oxa-10-phosphaphenanthrene-10-oxide (DOPO) dissolved in 20 mL of CH_2Cl_2 into another solution of the proper anhydrous manganese or zinc salt MX_2 (1.0 mmol, 0.126 g for $MnCl_2$, 0.215 g for $MnBr_2$, 0.309 g for MnI_2, 0.225 g for $ZnBr_2$) dissolved in 20 mL of EtOH. The reaction mixture was stirred inside the glove box overnight. The solution was concentrated under reduced pressure until a solid started to separate out. The product was then filtered, washed with diethyl ether (5 × 2 mL) and dried *in vacuo*. Yields: 75% (0.418 g) for $[MnCl_2(DOPO)_2]$, 79 % (0.511 g) for $[MnBr_2(DOPO)_2]$, 72% (0.534 g) for $[MnI_2(DOPO)_2]$, 81% (0.533 g) for for $[ZnBr_2(DOPO)_2]$. Crystals of $[ZnBr_2(DOPO)_2]$ suitable for X-ray diffraction were collected from toluene/ethanol solutions.

$[MnCl_2(DOPO)_2]$. Anal. calcd for $C_{24}H_{18}Cl_2MnO_4P_2$ (558.19 g mol^{-1}, %): C, 51.64; H, 3.25; Cl, 12.70. Found (%): C, 51.44; H, 3.26; Cl, 12.65. M.p. 190 °C. χ_M^{corr} (c.g.s.u.): $1.58{\cdot}10^{-2} \pm 0.09{\cdot}10^{-2}$. IR (KBr, cm^{-1}): 3060–3020 w (aromatic $\nu_{C\text{-}H}$), 2414 m ($\nu_{P\text{-}H}$), 1620–1560 w (aromatic $\nu_{C\text{-}C}$), 1240–1170 s ($\nu_{P=O}$ and $\nu_{C\text{-}O}$), 1044 w ($\nu_{P\text{-}O}$). UV–vis (EtOH, r.t., nm): 294, 267, 259, < 235 DOPO absorptions. PL (solid, r.t., $\lambda_{excitation}$ = 325 nm, nm): 635 ^{3}LC. PL (solid, r.t., $\lambda_{excitation}$ = 440 nm, nm): 535 $^4T_1(^4G)\rightarrow{}^6A_1(^6S)$, 635 ^{3}LC. PLE (solid, r.t., $\lambda_{emission}$ = 640 nm, nm): 405–470 $^4G\leftarrow{}^6A_1(^6S)$, < 400 DOPO excitation and $^4P,^4D,^4F\leftarrow{}^6A_1(^6S)$. PLE (solid, r.t., $\lambda_{emission}$ = 500 nm, nm): 405–470 $^4G\leftarrow{}^6A_1(^6S)$, 335–400 $^4P,^4D\leftarrow{}^6A_1(^6S)$. τ(solid, r.t., $\lambda_{excitation}$ = 290 nm, $\lambda_{emission}$ = 650 nm, ms): 8.2 (average). Φ(solid, r.t., $\lambda_{excitation}$ = 365 nm): 65%. Φ (solid, r.t., $\lambda_{excitation}$ = 310 nm): 60%.

$[MnBr_2(DOPO)_2]$. Anal. calcd for $C_{24}H_{18}Br_2MnO_4P_2$ (647.10 g mol^{-1}, %): C, 44.55; H, 2.80; Br, 24.70. Found (%): C, 44.37; H, 2.81; Br, 24.60. M.p. 210 °C. χ_M^{corr} (c.g.s.u.): $1.43{\cdot}10^{-2} \pm 0.08{\cdot}10^{-2}$. IR (KBr, cm^{-1}): 3060–3020 w (aromatic $\nu_{C\text{-}H}$), 2427 m ($\nu_{P\text{-}H}$), 1620–1560 w (aromatic $\nu_{C\text{-}C}$), 1212–1199 s ($\nu_{P=O}$ and $\nu_{C\text{-}O}$), 1044 w ($\nu_{P\text{-}O}$). UV–vis (EtOH, r.t., nm): 294, 267, 259, < 235 DOPO absorptions. PL (solid, r.t., $\lambda_{excitation}$ = 325 nm, nm): 536 $^4T_1(^4G)\rightarrow{}^6A_1(^6S)$, 625 ^{3}LC. PL (solid, r.t., $\lambda_{excitation}$ = 440 nm, nm): 536 $^4T_1(^4G)\rightarrow{}^6A_1(^6S)$, 625 ^{3}LC. PLE (solid, r.t., $\lambda_{emission}$ = 625 nm, nm): 415–505 $^4G\leftarrow{}^6A_1(^6S)$, 345–415 $^4P,^4D\leftarrow{}^6A_1(^6S)$, < 340 DOPO excitation and $^4F\leftarrow{}^6A_1(^6S)$. PLE (solid, r.t., $\lambda_{emission}$ = 505 nm, nm): 415–480 $^4G\leftarrow{}^6A_1(^6S)$, 345–415 $^4P,^4D\leftarrow{}^6A_1(^6S)$, < 340 DOPO excitation and $^4F\leftarrow{}^6A_1(^6S)$. τ (solid, r.t., $\lambda_{excitation}$ = 290 nm, $\lambda_{emission}$ = 505 nm, μs): 83. τ (solid, r.t., $\lambda_{excitation}$ = 290 nm, $\lambda_{emission}$ = 650 nm, ms): 35.2. Φ (solid, r.t., $\lambda_{excitation}$ = 365 nm): 77%. Φ (solid, r.t., $\lambda_{excitation}$ = 310 nm): 69%.

$[MnI_2(DOPO)_2]$. Anal. calcd for $C_{24}H_{18}I_2MnO_4P_2$ (741.10 g mol^{-1}, %): C, 38.90; H, 2.45; I, 34.25. Found (%): C, 38.74; H, 2.46; I, 34.11. M.p. 80 °C. χ_M^{corr} (c.g.s.u.): $1.52{\cdot}10^{-2} \pm 0.08{\cdot}10^{-2}$. IR (KBr, cm^{-1}): 3060–3020 w (aromatic $\nu_{C\text{-}H}$) 2410 m ($\nu_{P\text{-}H}$), 1620–1560 w (aromatic $\nu_{C\text{-}C}$), 1240–1170 s ($\nu_{P=O}$ and $\nu_{C\text{-}O}$), 1044 w ($\nu_{P\text{-}O}$). UV–vis (EtOH, r.t., nm): 294, 267, 259, < 235 DOPO absorptions. PL (solid, r.t., $\lambda_{excitation}$ = 325 nm, nm): 538 $^4T_1(^4G)\rightarrow{}^6A_1(^6S)$, 640 ^{3}LC. PL (solid, r.t., $\lambda_{excitation}$ = 440 nm, nm): 538 $^4T_1(^4G)\rightarrow{}^6A_1(^6S)$, 640 ^{3}LC. PLE (solid, r.t., $\lambda_{emission}$ = 640 nm, nm): 425–515 $^4G\leftarrow{}^6A_1(^6S)$, 355–420 $^4P,^4D\leftarrow{}^6A_1(^6S)$, < 350 DOPO excitation and $^4F\leftarrow{}^6A_1(^6S)$. PLE (solid, r.t., $\lambda_{emission}$ = 510 nm, nm): 425–480 $^4G\leftarrow{}^6A_1(^6S)$, 355–420 $^4P,^4D\leftarrow{}^6A_1(^6S)$, < 350 DOPO excitation and $^4F\leftarrow{}^6A_1(^6S)$. τ (solid, r.t., $\lambda_{excitation}$ = 290 nm, $\lambda_{emission}$ = 505 nm, μs): 13. τ (solid, r.t., $\lambda_{excitation}$ = 290 nm, $\lambda_{emission}$ = 650 nm, ms): 15.3. Φ (solid, r.t., $\lambda_{excitation}$ = 365 nm): 18%. Φ (solid, r.t., $\lambda_{excitation}$ = 310 nm): 20%.

$[ZnBr_2(DOPO)_2]$. Anal. calcd for $C_{24}H_{18}Br_2O_4P_2Zn$ (657.54 g mol^{-1}, %): C, 43.84; H, 2.76; Br, 24.30. Found (%): C, 43.68; H, 2.77; Br, 24.21. M.p. 175 °C (dec.). ^1H NMR ($CDCl_3$, 213 K) δ 8.27 (d, 1H, $^1J_{PH}$ = 620 Hz, P—H), 8.07 (dd, 1H, J_{PH} = 15.8 Hz, J_{HH} = 7.6 Hz, H_1), 8.02 (dd, 1H, J_{HH} = 8.1 Hz, J_{PH} = 5.6 Hz, H_4), 7.96 (dd, 1H, J_{HH} = 8.1 Hz, J_{HH} = 1.6 Hz, H_5), 7.80 (t, 1H, J_{HH} = 7.7 Hz, H_3), 7.58 (td, 1H, J_{HH} = 7.7 Hz, J_{PH} = 2.9 Hz, H_2), 7.44 (t, 1H, J_{HH} = 7.7 Hz, H_7), 7.37–7.27 (m, 2H, $H_{6,8}$). $^{31}P\{^1H\}$ NMR ($CDCl_3$, 213 K) δ 19.44 (FWHM = 35 Hz). IR (KBr, cm^{-1}): 3100–3015 w (aromatic $\nu_{C\text{-}H}$), 2418 m ($\nu_{P\text{-}H}$), 1640–1560 m (aromatic $\nu_{C\text{-}C}$), 1220–1190 s ($\nu_{P=O}$ and $\nu_{C\text{-}O}$), 1047 w ($\nu_{P\text{-}O}$). UV–vis

(EtOH, r.t., nm): 294, 267, 259, < 235 DOPO absorptions. PL (solid, r.t., $\lambda_{excitation}$ = 280 nm, nm): 380 ^{1}LC, 632 ^{3}LC. PLE (solid, r.t., $\lambda_{emission}$ = 630 nm, nm) < 370 DOPO excitation. T(solid, r.t., $\lambda_{excitation}$ = 373 nm, $\lambda_{emission}$ = 405 nm,ns): 4; τ(solid, r.t., $\lambda_{excitation}$ = 290 nm, $\lambda_{emission}$ = 630 nm, ms): 8.2. Φ(solid, r.t., $\lambda_{excitation}$ = 310 nm): 11%.

2.3. Crystal structure determination and powder XRD measurements

The crystallographic data were collected at CACTI (Universidade de Vigo) at 100 K (CryoStream 800) using a Bruker D8 Venture Photon II CMOS detector and Mo-Kα radiation (λ = 0.71073 Å) generated by an Incoatec high brilliance IμS microsource. The software APEX3 [59] was used for collecting frames of data, indexing reflections, and the determination of lattice parameters, SAINT [59] for integration of the intensity of reflections, and SADABS [59] for scaling and empirical absorption correction. The crystallographic treatment was performed using the Oscail program [60], solved using the SHELXT program [61]. The structure was subsequently refined by a full-matrix least-squares methods based on F^2 using the SHELXL program [62]. Non-hydrogen atoms were refined with anisotropic displacement parameters. Treatment of the hydrogen atoms was mixed, those bonded to the phosphorus atoms were found in the final electronic density and refined isotropically. The other ones were calculated on the basis of a riding model. Other details concerning crystal data and structural refinement are given in Table 1. CCDC 2,177,563 contains the supplementary crystallographic data for this paper. These data can be obtained free of charge from the Cambridge Crystallographic Data Centre via https://www.ccdc.cam.ac.uk/data_request/cif. PLATON (version 290122) [63] was used to obtain some geometrical parameters from the cif file.

Powder XRD measurements were carried out using Cu-Kα radiation with a Malvern Pananalytical Empyrean instrument equipped with a PIXcel3D-Medipix3 1x1 detector. The scan range was set from 4.0 to 101.0°.

Table 1
Crystal data and structure refinement for [$ZnBr_2(DOPO)_2$].

Empirical formula	C_{24} H_{18} Br_2 O_4 P_2 Zn
Formula weight	657.51
Temperature	100(2) K
Wavelength	0.71073 Å
Crystal system	Triclinic
Space group	*P*-1
Unit cell dimensions	a = 7.4593(3) Å b = 9.8654(4) Å c = 16.7638(8) Å α = 85.436(2)° β = 87.870(2)° γ = 70.289(2)°
Volume	1157.59(9) Å^3
Z	2
Density (calculated)	1.886 Mg/m^3
Absorption coefficient	4.682 mm^{-1}
F(000)	648
Crystal size	0.275 × 0.213 × 0.188 mm
Theta range for data collection	2.198 to 28.297°
Index ranges	$-9 \le h \le 9$ $-13 \le k \le 13$ $-22 \le l \le 22$
Reflections collected	59,106
Independent reflections	5737 [R_{int} = 0.0559]
Reflections observed (>2σ)	5339
Data Completeness	0.999
Absorption correction	Semi-empirical from equivalents
Max. and min. transmission	0.7457 and 0.5188
Refinement method	Full-matrix least-squares on F^2
Data / restraints / parameters	5737 / 0 / 306
Goodness-of-fit on F^2	1.051
Final *R* indices [$I > 2\sigma(I)$]	R_1 = 0.0207 wR_2 = 0.0485
R indices (all data)	R_1 = 0.0233 wR_2 = 0.0496
Largest diff. peak and hole	0.558 and −0.422 e.Å^{-3}

2.4. Computational details

The computational geometry optimizations of [$ZnBr_2(DOPO)_2$] (singlet and triplet states) were carried out without symmetry constraints, using the global-hybrid *meta*-NGA functional MN15 [64] and the def2 split-valence polarized basis set of Ahlrichs and Weigend [65]. The C-PCM implicit solvation model was added to MN15 calculations (ε = 9.08) [66,67]. The "unrestricted" formalism was applied in the presence of unpaired electrons and the absence of meaningful spin contamination was verified by comparing the computed $< S^2 >$ values with the theoretical ones [68]. The relative energies of the [$ZnBr_2(DOPO)_2$] excited states were obtained by carrying out TD-DFT (time-dependent DFT) calculations at the same theoretical level, starting from singlet and triplet state geometries [69]. The software used was Gaussian 16 [70] and the output files were analysed with Multiwfn, version 3.5 [71]. Cartesian coordinates of the DFT-optimized structures are provided in the Supporting Information.

3. Results and discussion

3.1. Synthesis of the complexes and X-ray structure determination of [$ZnBr_2(DOPO)_2$]

Complexes having general formula [$MX_2(DOPO)_2$] (M = Mn, X = Cl, Br, I; M = Zn, X = Br; DOPO = 9,10-dihydro-9-oxa-10-phosphaphenanthrene-10-oxide) were easily synthesized by reacting the proper anhydrous MX_2 salt with two equivalents of DOPO at room temperature in ethanol/dichloromethane solution. The proposed formulae were confirmed by elemental analysis data. The experimental magnetic moments of the Mn(II) complexes are in line with the theoretical 5.9 BM expected for high-spin d^5 derivatives of first-row transition elements (see Table S1 for magnetic susceptibility data ad diamagnetic corrections). No resonance attributable to the presence of diamagnetic species was observed in the $^{31}P\{^1H\}$ NMR spectra of [$MnX_2(DOPO)_2$] complexes. On the other hand, the ^1H and $^{31}P\{^1H\}$ NMR spectra of the diamagnetic [$ZnBr_2(DOPO)_2$] derivative recorded at variable temperature revealed fluxional behaviour in $CDCl_3$ solution, as clearly observable from the comparison with the NMR spectra of free DOPO (Fig. 1 and Figure S1). The eight aromatic ^1H resonances expected for two equivalent coordinated DOPO ligands can be however detected, and the $^1J_{PH}$ coupling constant raises from the 593 Hz of free DOPO to 620 Hz in [$ZnBr_2(DOPO)_2$]. It is likely to suppose that the donation of electronic density from DOPO to Zn(II) makes the phosphorus atom more electrophilic and strengthens the P—H bond. The $^{31}P\{^1H\}$ NMR resonance of [$ZnBr_2(DOPO)_2$] is shifted at higher frequency with respect to the free ligand by about 5 ppm and the singlet is much broader.

The IR spectra of the [$MX_2(DOPO)_2$] complexes are roughly superimposable, as observable for instance in Fig. 2, reporting those of [$MnBr_2(DOPO)_2$] and [$ZnBr_2(DOPO)_2$]. The $\nu_{P\text{-}H}$ stretchings [72] fall at slightly higher wavenumbers in the [$MX_2(DOPO)_2$] complexes with respect to the free ligand (Fig. 2), a result in line with the increased $^1J_{PH}$ coupling constant in [$ZnBr_2(DOPO)_2$] with respect to DOPO. DFT calculations on DOPO and [$ZnBr_2(DOPO)_2$] confirmed the shortening of the P-H bond, from 1.403 Å in the free ligand to the average value of 1.397 Å in the complex. The $\nu_{P=O}$ stretchings are present in the 1250–1150 cm^{-1} range, superimposed to other vibrations. Despite the difficulty in the precise assignment of the $\nu_{P=O}$ stretchings, the comparison with free DOPO suggests a slight weakening of the P=O bonds caused by coordination, as already observed for comparable species [38,39,73].

Thermogravimetric analyses revealed in all the cases no weight loss below 170 °C, supporting the idea that no coordinated solvent molecules are present. The TGA curves are shown in Figure S2.

All the characterization data suggest the formation of four-coordinated mononuclear complexes, similarly to what was observed

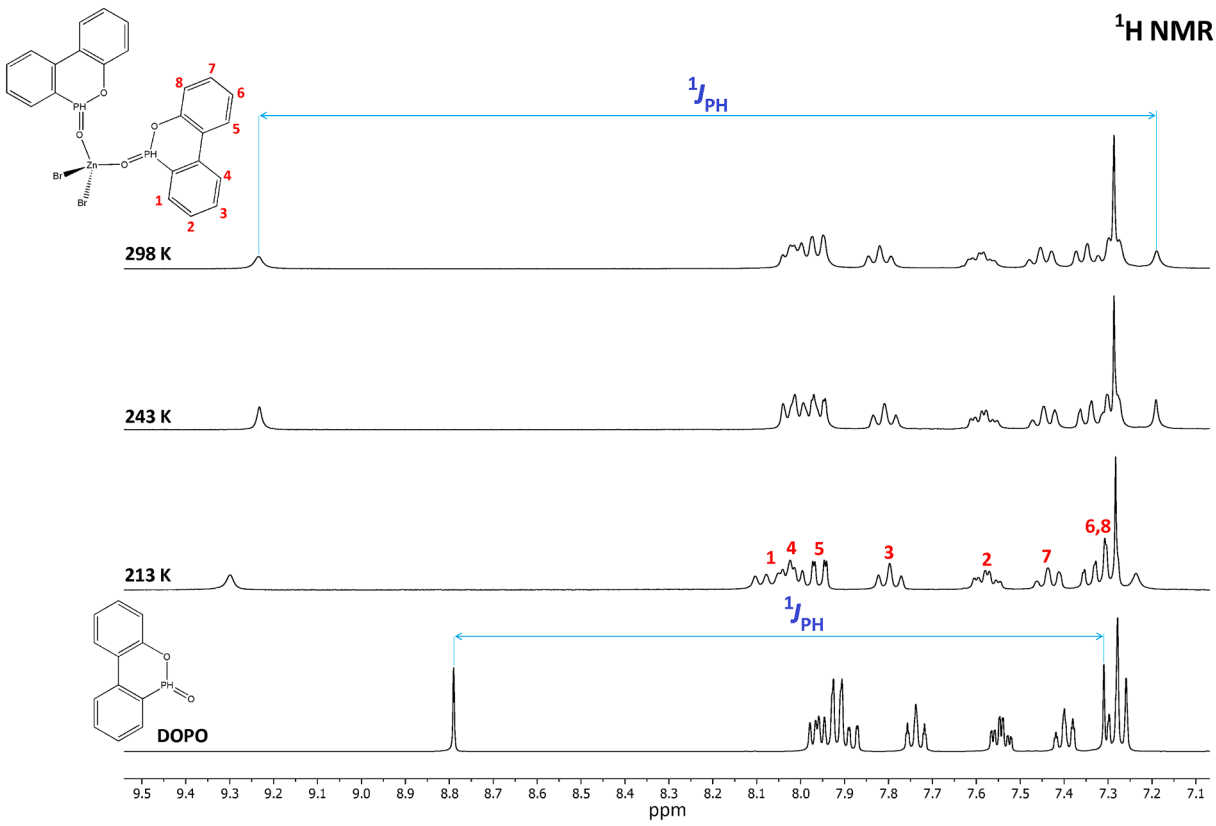

Fig. 1. ^{1}H NMR spectra at variable temperature of $[ZnBr_2(DOPO)_2]$ and of free DOPO in $CDCl_3$.

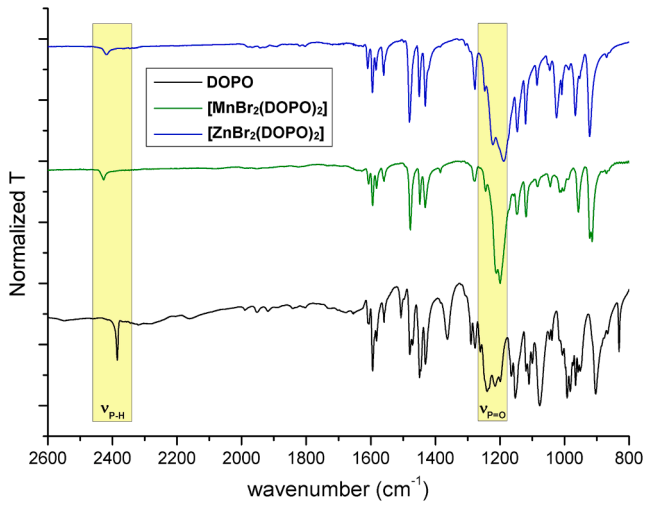

Fig. 2. IR spectra (KBr pellet) of $[MBr_2(DOPO)_2]$ (M = Mn, Zn) and of free DOPO.

for triphenylphosphine oxide once coordinated to Mn(II) and Zn(II) halides [74,75]. Such a hypothesis was further confirmed by the single-crystal X-ray structure of $[ZnBr_2(DOPO)_2]$. The Zn(II) ion is coordinated by two halogen atoms and two oxygen atoms from two DOPO ligands in a distorted tetrahedral geometry (see Fig. 3). In Table 2 the most significant distances and angles are set out. Bond lengths are comparable with those recently reported for the Zn(II) bromide complex with two *N*,*N*,*N*',*N*'-tetramethyl-*P*-indol-1-ylphosphonic diamide ligands in the coordination sphere [43], although the Zn-O distances are slightly shorter and, consequently, the Zn-Br bonds are slightly longer.

As mentioned in the Introduction section, zinc(II) compounds with [O=P]-donor ligands were poorly investigated under a structural point of view, and $[ZnBr_2(DOPO)_2]$ represents a new interesting example of this class of compounds. The distortion of the coordination tetrahedron around the metal centre can be described by the well-known τ_4 parameter, equal to 0.90 [76], or by the τ'_4 parameter, equal to 0.85 [77]. Both parameters are between the values related to the perfect tetrahedral environment (1.0) and the trigonal pyramidal (0.85). Continuous Shape Measures [78,79] indicate that the first coordination sphere is best defined as a tetrahedron, although deviated towards a vacant trigonal bipyramid (Table S2).

As occurs in $[ZnX_2\{O=P(NMe_2)_2Ar\}]$ (X = Br, I; Ar = 1-indolyl) derivatives, the X-Zn-X angle equal to 123.53(1)° is the most obtuse one, even bigger than the values in the previously mentioned compounds, that are around 120°, and also greater than the 117° found in $[ZnBr_2(O=PPh_3)]$ [75]. On the other hand the O-Zn-O angle equal to 98.16(5)° is smaller than those found in the previously mentioned compounds, where it was between 100.9 and 104.5°.

An interesting feature is the difference between the DOPO ligands coordinated to the metal centre. One of them is essentially planar and the dihedral angle between the two phenyl rings is only 3.3(1)°. Instead, the dihedral angle is equal to 14.9(1)° for the other ligand. Moreover, the $\{POC_4\}$ rings show some differences. In the planar ligand there is a scarce deviation from the planarity towards a screw-boat conformation with puckering parameters Q = 0.1423(14) Å, θ = 61.3(7)° and φ = 23.7 (8)° [80]. The same plane in the other ligand shows puckering parameters indicating significant ring wrinkling, Q = 0.4052(13) Å, θ = 115.1 (2) ° and φ = 204.4(3)° (see Figure S3). The P=O-Zn angles are also influenced by this different behaviour, in such a way that for the planar ligand the angle is 143.27(9)°, quite different with respect to the 134.80 (8)° found for the puckered ligand.

The supramolecular network is also affected by the planarity of the ligands (or vice versa), and the planar aromatic systems allow an infinite face-to-face π, π '-stacking interaction. The distances between centroids

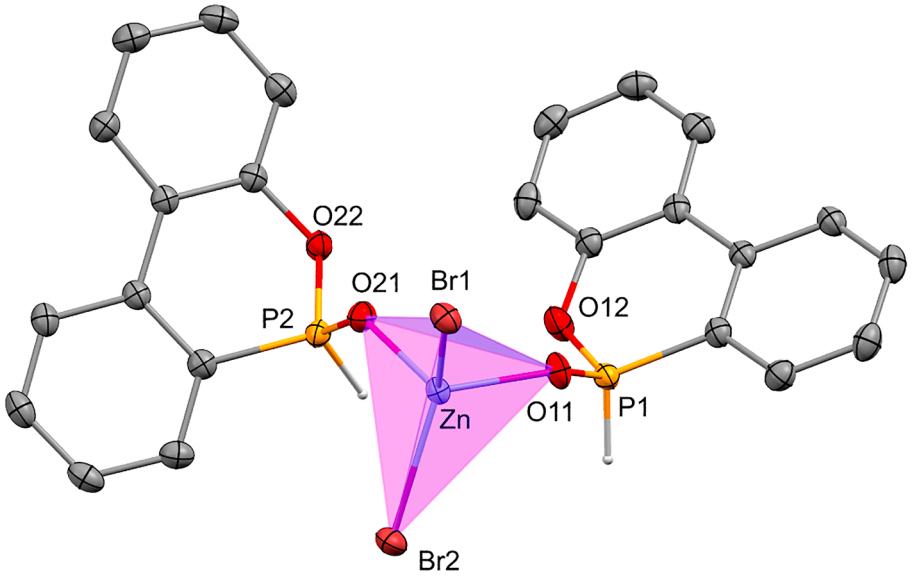

Fig. 3. X-ray structure of $[ZnBr_2(DOPO)_2]$. Only the P-bonded hydrogen atoms are shown.

Table 2
Selected bond lengths [Å] and angles [°] for $[ZnBr_2(DOPO)_2]$.

Zn-O(11)	1.9975(12)	Zn-O(21)	1.9952(12)
Zn-Br(1)	2.3489(3)	Zn-Br(2)	2.3379(3)
P(1)-O(11)	1.4851(13)	P(2)-O(21)	1.4907(13)
P(1)-O(12)	1.5761(14)	P(2)-O(22)	1.5812(13)
P(1)-C(11)	1.7668(18)	P(2)-C(21)	1.7661(18)
O(11)-Zn-O(21)	98.16(5)	Br(2)-Zn-Br(1)	123.531(11)
O(21)-Zn-Br(1)	109.61(4)	O(21)-Zn-Br(2)	105.91(4)
O(11)-Zn-Br(1)	106.51(4)	O(12)-Zn-Br(2)	110.20(4)
O(11)-P(1)-O(12)	114.68(8)	O(21)-P(2)-O(22)	112.04(7)
O(11)-P(1)-C(12)	112.51(8)	O(21)-P(2)-C(21)	115.26(8)
O(12)-P(1)-C(11)	105.56(8)	O(22)-P(2)-C(21)	103.90(7)
C(112)-O(12)-P(1)	126.34(12)	C(212)-O(22)-P(2)	119.72(11)
P(1)-O(11)-Zn	143.27(9)	P(2)-O(21)-Zn	134.80(8)

are 3.7418(13) Å with the molecule situated below and 3.7680(13) Å with the one situated above (see Figure S4). The dihedral angles between planes are 3.26(10)°. The other coordinated DOPO ligands show stacking interactions too, but not as a ladder, because the molecule situated below interacts only through one of the phenyl rings, with distances between centroids of only 3.6980(11) Å (both planes are parallel for symmetry reasons). Above the plane the interaction is again face to face, with slightly longer distances between centroids equal to 3.8121(12) Å, but dihedral angles between planes of 14.86(10)° (see Figure S5).

Powder XRD experiment was carried out on $[ZnBr_2(DOPO)_2]$ in order to establish its crystalline phase purity. As shown in Figure S6, the powder XRD pattern of the bulk sample is consistent with the simulated pattern based on the single-crystal data, indicating the presence of one crystalline phase in the prepared solid. Powder XRD experiments were also carried out on $[MnX_2(DOPO)_2]$ complexes to check if the zinc and manganese derivatives have comparable space group and cell parameters. As shown in Figure S7, the powder XRD patterns for $[ZnBr_2(DOPO)_2]$ and $[MnBr_2(DOPO)_2]$ are indicative of different cell parameters, and the same conclusion was reached on comparing the powder XRD patterns for $[MnCl_2(DOPO)_2]$ and $[MnBr_2(DOPO)_2]$ (Figure S8). Such a result is not surprising, since other $[MnX_2L_2]$ studied by our group gave different cell parameters on changing the halogen atom [45].

3.2. Absorption and emission properties of the complexes

All the complexes show absorptions in solution for wavelengths below 325 nm comparable to those of free DOPO, as observable from the superimposition of the spectra in Figure S9. The TD-DFT computed hole and electron distributions for the lowest energy singlet ← singlet absorption of $[ZnBr_2(DOPO)_2]$ ($\lambda_{predicted}$ = 272 nm) confirm that the transition involves the π-conjugated system of the DOPO ligands (Figure S9). The $[MX_2(DOPO)_2]$ complexes at the solid state exhibit appreciable luminescence in the visible range upon excitation with UV light, not maintained in solution. No triboluminescence was detected. The photoluminescence quantum yield (Φ) values are around 70% for $[MnCl_2(DOPO)_2]$ and $[MnBr_2(DOPO)_2]$ and between 10% and 20% for $[MnI_2(DOPO)_2]$ and $[ZnBr_2(DOPO)_2]$. The Φ values for the Mn(II) derivatives were measured using $\lambda^{max}_{excitation}$ = 310 and 365 nm, but the variations resulted negligible. The determination of the Φ value for $[ZnBr_2(DOPO)_2]$ was instead limited to $\lambda^{max}_{excitation}$ = 310 because of the presence of an emission centred in the near-UV range (*vide infra*). The PL spectra of the Mn(II) derivatives show two bands, the first one in the green region attributable to the $^4T_1(^4G)\rightarrow{}^6A_1(^6S)$ transition of the metal ion in tetrahedral environment, and the other one centred in the red region of the spectrum with maximum comprised between 625 and 640 nm. The relative intensity of the two bands depends upon the choice of the halide and the excitation wavelength. As observable in Fig. 4 (see Figure S10 for the 3D PL spectrum), the red emission (FWHM around 3500 cm^{-1}) dominates the PL spectrum of $[MnCl_2(DOPO)_2]$ and the $^4T_1(^4G)\rightarrow{}^6A_1(^6S)$ transition is detectable only by direct excitation of Mn (II). Such a wavelength-dependent behaviour is more pronounced for $[MnBr_2(DOPO)_2]$ (Figs. 4 and 5). The red emission is the most intense only for short excitation wavelengths, while the two bands assume comparable intensity for $\lambda_{excitation} > 380$ nm. Finally, the PL spectrum of $[MnI_2(DOPO)_2]$ is composed by two bands with relative intensity almost independent upon the excitation wavelength (Figures 4 and S11). The PLE spectra (see Fig. 5 and Figures S10-S11) indicate that the emissions in the green region are mainly associated to the direct Mn(II) excitation, in particular the $^4G^4D,^4P\leftarrow{}^6S$ transitions for wavelengths longer than 330 nm. On the other hand, the emission band in the red range appears mostly associated to the excitation of the coordinated ligands, even if PLE bands related to Mn(II) transitions are observable.

The hypothesis that the luminescence at longer wavelengths is not related to Mn(II) transitions is supported by the emission spectrum of $[ZnBr_2(DOPO)_2]$ (Fig. 6), that shows a band with maximum at 632 nm

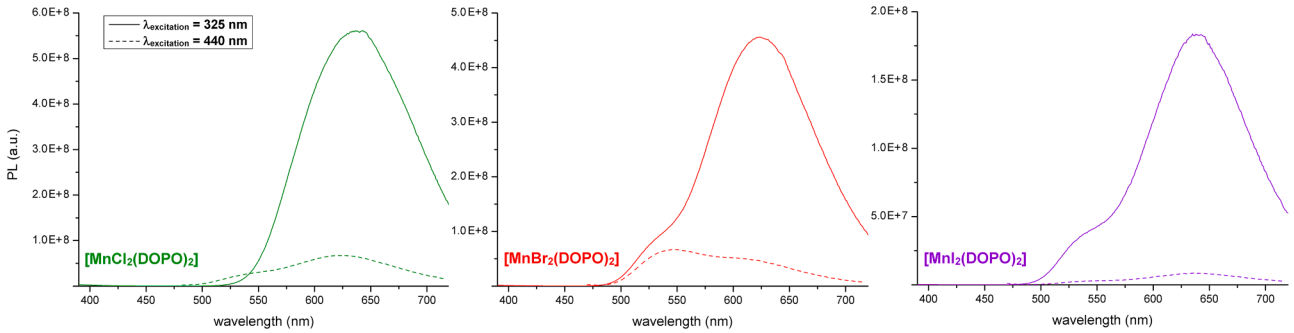

Fig. 4. PL spectra of $[MnX_2(DOPO)_2]$ complexes (X = Cl, green; X = Br, red; X = I, violet). Solid samples, r.t., $\lambda_{excitation}$ = 325 nm (solid line) and $\lambda_{excitation}$ = 440 nm (dashed line).

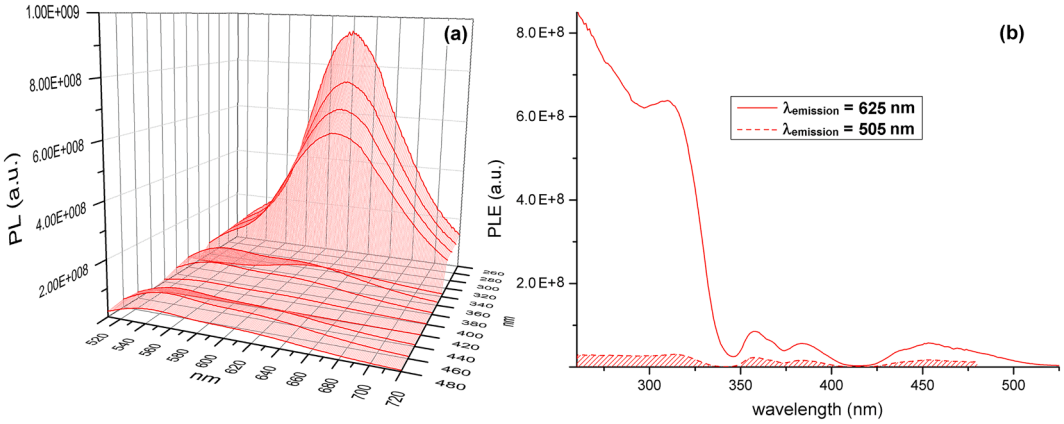

Fig. 5. (a) 3D PL spectrum of $[MnBr_2(DOPO)_2]$. (b) PLE spectra of $[MnBr_2(DOPO)_2]$ complexes, $\lambda_{emission}$ = 625 nm (solid line) and $\lambda_{emission}$ = 505 nm (dashed line). Solid samples, r.t.

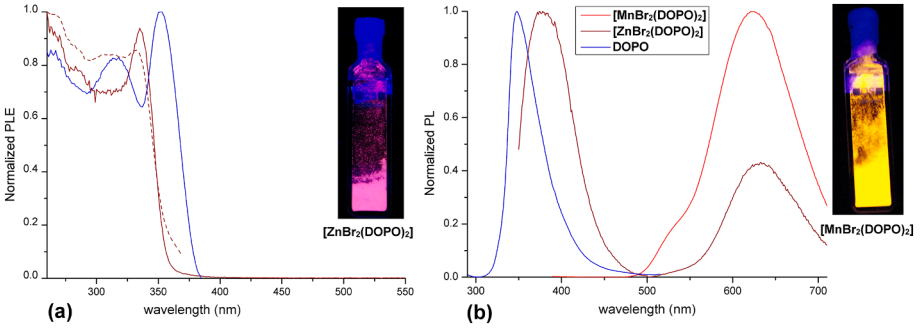

Fig. 6. (a) PLE spectra of DOPO (blue line, $\lambda_{emission}$ = 430 nm) and $[ZnBr_2(DOPO)_2]$ (wine lines: solid line, $\lambda_{emission}$ = 630 nm; dashed line, $\lambda_{emission}$ = 390 nm). (b) PL spectra of of DOPO (blue line, $\lambda_{excitation}$ = 270 nm), $[MnBr_2(DOPO)_2]$ (red line, $\lambda_{excitation}$ = 325 nm) and $[ZnBr_2(DOPO)_2]$ (wine line, $\lambda_{excitation}$ = 325 nm). Solid samples, r.t. Insets: pictures of $[MBr_2(DOPO)_2]$ (M = Mn, Zn) complexes excited at 365 nm.

strictly comparable to that of the analogous Mn(II) derivative. Another emission band of $[ZnBr_2(DOPO)_2]$ centred in the near-UV range is present, similar to that recorded for free DOPO. The maximum is slightly shifted at longer wavelengths probably because of the stabilization of DOPO excited states caused by coordination to Zn(II). The dual emission from $[ZnBr_2(DOPO)_2]$ is observable by using excitation wavelengths in almost all the UV range (see also Figure S12). On the other hand, the emission of the free ligand does not depend upon the excitation wavelength, as observable in Figure S12. The lifetime of this emission is around 4 ns and the same value was measured for free DOPO, accordingly to a fluorescent emission (see Figure S13 for the luminescence decay curves). The fluorescence from coordinated DOPO is completely quenched in Mn(II) derivatives, indicating faster intersystem crossing and energy transfer with respect to $[ZnBr_2(DOPO)_2]$. The presence of the fluorescence band in the PL spectrum of $[ZnBr_2(DOPO)_2]$ causes a strong variation of the colour of the emission with respect to the related Mn(II) derivative, as observable in Fig. 6. On the other hand, the PLE spectra of $[ZnBr_2(DOPO)_2]$ (Fig. 6) are comparable to those of the Mn(II) complexes, with the expected lack of bands related to the direct excitation of the metal centre. The PLE spectrum of free DOPO is also roughly similar in the 260 – 336 nm range, while for longer wavelengths the superimposition of the emission band is clearly observable (Fig. 6).

It is likely to suppose that in all the $[MX_2(DOPO)_2]$ complexes the band in the red range is caused by an emission from triplet states localized on the DOPO ligands (^{3}LC), in line with previous outcomes on $[MnX_2\{O{=}P(NMe_2)_2Ar\}_2]$ derivatives (X = halides; Ar = 2-naphthyl, 1-

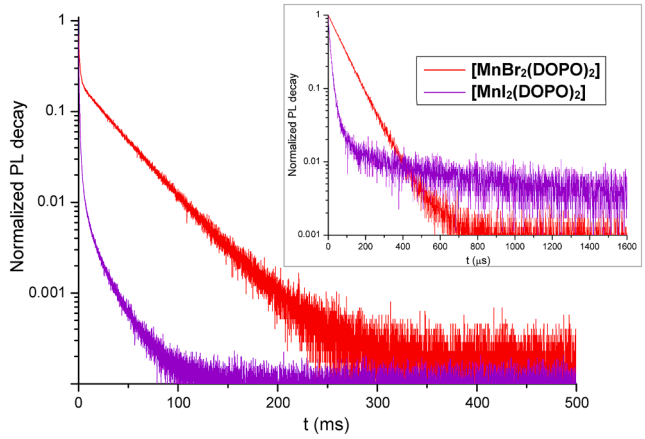

Fig. 7. Normalized plots of the luminescence decay curves of $[MnBr_2(DOPO)_2]$ (red line) and $[MnI_2(DOPO)_2]$ (violet line). Solid samples, r.t., $\lambda_{excitation}$ = 290 nm, $\lambda_{emission}$ = 650 nm. Inset: $\lambda_{emission}$ = 505 nm.

carbazolyl) [44,45]. Moreover, ^{3}LC emission was recently reported by our research group for $[ZnX_2\{O{=}P(NMe_2)_2Ar\}_2]$ (X = Br, I; Ar = 1-indolyl) [43]. Accordingly, a long component in the luminescence decay curves was observed for all the $[MX_2(DOPO)_2]$ derivatives, falling in the milliseconds range (Figure S14). Such a decay is superimposed to a faster process, particularly evident for $[MnBr_2(DOPO)_2]$ and $[MnI_2(DOPO)_2]$ (Fig. 7), associated to the metal-centred emission process. The fast component of the luminescence decay curves of $[MnBr_2(DOPO)_2]$ and $[MnI_2(DOPO)_2]$, measured at $\lambda_{emission}$ = 505 nm, has estimated lifetime in the tenths of μs range (about 83 μs for $[MnBr_2(DOPO)_2]$ and 13 μs for $[MnI_2(DOPO)_2]$), as expected for tetrahedral Mn(II) derivatives [22,23]. Unfortunately, we were unable to measure the lifetime related to the green emission of $[MnCl_2(DOPO)_2]$ because of its poor relative intensity with the available pulsed excitation sources.

The ^{3}LC nature of the emission in the red region was supported by TD-DFT calculations on the optimized structure of $[ZnBr_2(DOPO)_2]$ (triplet state). The hole and electron distributions for the emission ($\lambda_{predicted}$ = 578 nm) show that the transition is localized of the π-delocalized orbitals of the coordinated DOPO ligands (Figure S14). As occurs for the ground-state singlet geometries, the computed P-H bonds are shorter in the optimized triplet geometry of $[ZnBr_2(DOPO)_2]$ (average value 1.401 Å) with respect to the triplet geometry of free DOPO (1.411 Å) because of the coordination to $ZnBr_2$. The singlet–triplet energy gap is also influenced by coordination, lowering from the 2.22 eV of free DOPO to the 2.14 eV of the Zn(II) complex. It is however worth noting that the decays shown in Figure S14 are not directly related to the increased spin–orbit coupling in the presence of heavier halides, a result particularly evident on considering the Mn(II) derivatives. Despite that the emission is the red range is supposed to be ligand-centred and therefore the nature of the halides should have a minor role, the decay should become more rapid on increasing the atomic number of the halide. A possible hypothesis is that the complexes here considered have different intermolecular interactions at the solid state, influencing the excited state lifetimes.

The excitation wavelength-dependent behaviour of the Mn(II) complexes can be rationalized following the approach proposed for $[MnX_2\{O{=}P(NMe_2)_2(carbazolyl)\}_2]$ derivatives [45], based on the increased spin–orbit coupling moving from X = Cl to X = I [81]. The ligand–metal energy transfer is probably slow in $[MnCl_2(DOPO)_2]$, therefore the ^{3}LC emission is favoured on exciting the coordinated DOPO and the $^4T_1(^4G)\rightarrow{}^6A_1(^6S)$ transition is detectable only by direct excitation of the Mn(II) centre, with relatively weak PLE bands. The same energy transfer is faster in $[MnBr_2(DOPO)_2]$, but emission spectra with different relative intensities of the $^4T_1(^4G)\rightarrow{}^6A_1(^6S)$ and ^{3}LC transitions are observable if the ligands or the metal are preferentially excited. Finally, the ligand–metal energy transfer in $[MnI_2(DOPO)_2]$ is probably so fast that the emission spectrum becomes independent upon the excitation wavelength.

4. Conclusions

The results here described show that the commercially available *H*-phosphinate DOPO behaves as O-donor ligand towards Mn(II) and Zn(II) centres, with the straightforward formation of halide complexes having general formula $[MX_2(DOPO)_2]$. The coordinating behaviour appears comparable to that of phosphine oxides, phosphoramides and phosphonates, despite the different formal oxidation state of the phosphorous atom. The photoluminescence of the isolated coordination compounds is characterized by triplet ligand-centred transitions, as already observed on considering arylphosphonic diamides with π-delocalized fragments as ligands.

The results provided in the present paper, compared with recent outcomes on related species, point out that the introduction of π-conjugated systems in [O=P]-donor ligands shifts the luminescence of the corresponding Mn(II) halide complexes from metal-centred to ligand-centred emission. Excitation wavelength-dependent behaviour is observable, depending upon the choice of the coordinated halides. Finally, π-delocalized [O=P]-donor ligands appear suitable for the isolation of quite unusual phosphorescent Zn(II) halide complexes.

Further studies on the coordination compounds here reported will be carried out focusing the attention on their potential behaviour as flame retardants in polymer matrices. The aim of the future investigations is the preparation of multifunctional materials combining photoluminescent and flame retardant features.

Declaration of Competing Interest

The authors declare that they have no known competing financial interests or personal relationships that could have appeared to influence the work reported in this paper.

Acknowledgements

Università Ca' Foscari Venezia is gratefully acknowledged for financial support (Bando Spin 2018, D. R. 1065/2018 prot. 67416). CACTI (University of Vigo) and Cineca (Bologna) are gratefully acknowledged for X-ray data collection and availability of high-performance computer resources (class C project COLUMN21). We sincerely thank Tiziano Finotto (Università Ca' Foscari Venezia) for the powder XRD measurements.

References

[1] X. Song, H. Xu, Pure-organic phosphine oxide luminescent materials, J. Inf. Disp. 21 (2020) 149–172, https://doi.org/10.1080/15980316.2020.1788657.
[2] C.C. Kenry, B. Liu, Enhancing the performance of pure organic room-temperature phosphorescent luminophores, Nat. Commun. 10 (2019) 2111, https://doi.org/10.1038/s41467-019-10033-2.
[3] D. Kim, S. Salman, V. Coropceanu, E. Salomon, A.B. Padmaperuma, L.S. Sapochak, A. Kahn, J.-L. Brédas, Phosphine Oxide Derivatives as Hosts for Blue Phosphors: A Joint Theoretical and Experimental Study of Their Electronic Structure, Chem. Mater. 22 (2010) 247–254, https://doi.org/10.1021/cm9029616.
[4] P. She, J. Duan, J. Lu, Y. Qin, F. Li, C. Liu, S. Liu, Y. Ma, Q. Zhao, Single-component molecular dual persistent room temperature phosphorescence from low- and high-

lying triplet states, Adv. Optical Mater. 10 (2022) 2102706, https://doi.org/10.1002/adom.202102706.
[5] C. Liu, Y. Gu, Q. Fu, N. Sun, C. Zhong, D. Ma, J. Qin, C. Yang, Nondoped deep-blue organic light-emitting diodes with color stability and very low efficiency roll-off: solution-processable small-molecule fluorophores by phosphine oxide linkage, Chem. Eur. J. 18 (2012) 13828–13835, https://doi.org/10.1002/chem.201201512.
[6] Z. Zhao, G. Yu, Q. Chang, X. Liu, Y. Liu, L. Wang, Z. Liu, Z. Bian, W. Liu, C. Huang, Carbazolylphosphines and carbazolylphosphine oxides: facilely synthesized host materials with tunable mobilities and high triplet energy levels for blue phosphorescent OLEDs, J. Mater. Chem. C 5 (2017) 7344–7351, https://doi.org/10.1039/C7TC01594A.
[7] A. Wada, T. Yasuda, Q. Zhang, Y. Seok Yang, I. Takasu, S. Enomoto, C. Adachi, A host material consisting of a phosphinic amide directly linked donor–acceptor structure for efficient blue phosphorescent organic light-emitting diodes, J. Mater. Chem. C 1 (2013) 2404–2407, https://doi.org/10.1039/C3TC00939D.
[8] Y. Tao, J. Xiao, C. Zheng, Z. Zhang, M. Yan, R. Chen, X. Zhou, H. Li, Z. An, Z. Wang, H. Xu, W. Huang, Dynamically adaptive characteristics of resonance variation for selectively enhancing electrical performance of organic semiconductors, Angew. Chem. 125 (2013) 10685–10689, https://doi.org/10.1002/ange.201304540.
[9] C. Liu, Y. Li, Y. Li, C. Yang, H. Wu, J. Qin, Y. Cao, Efficient solution-processed deep-blue organic light-emitting diodes based on multibranched oligofluorenes with a phosphine oxide center, Chem. Mater. 25 (2013) 3320–3327, https://doi.org/10.1021/cm401640v.
[10] C. Han, F. Zhao, Z. Zhang, L. Zhu, H. Xu, J. Li, D. Ma, P. Yan, Constructing low-triplet-energy hosts for highly efficient blue PHOLEDs: controlling charge and exciton capture in doping systems, Chem. Mater. 25 (2013) 4966–4976, https://doi.org/10.1021/cm403160p.
[11] C. Hippola, D. Danilovic, U. Bhattacharjee, C. Perez-Bolivar, K.A. Niradha Sachinthani, T.L. Nelson, P. Anzenbacher, J.W. Petrich, R. Shinar, J. Shinar, Bright Deep Blue TADF OLEDs: The role of triphenylphosphine oxide in NPB/TPBi:PPh3O exciplex emission, Adv. Optical Mater. 8 (2020) 1901282, https://doi.org/10.1002/adom.201901282.
[12] J. Wang, C. Liu, C. Jiang, C. Yao, M. Gu, W. Wang, Solution-processed aggregation-induced delayed fluorescence (AIDF) emitters based on strong π-accepting triazine cores for highly efficient nondoped OLEDs with low efficiency roll-off, Org. Electron. 65 (2019) 170–178, https://doi.org/10.1016/j.orgel.2018.11.018.
[13] H.-B. Kim, J.-J. Kim, Recent progress on exciplex-emitting OLEDs, J. Inf. Disp. 20 (2019) 105–121, https://doi.org/10.1080/15980316.2019.1650838.
[14] J. Jia, L. Zhu, Y. Wei, Z. Wu, H. Xu, D. Ding, R. Chen, D. Ma, W. Huang, Triazine-phosphine oxide electron transporter for ultralow-voltage-driven sky blue PHOLEDs, J. Mater. Chem. C 3 (2015) 4890–4902, https://doi.org/10.1039/C4TC02993C.
[15] T.-T. Bui, F. Goubard, M. Ibrahim-Ouali, D. Gigmes, F. Dumur, Recent advances on organic blue thermally activated delayed fluorescence (TADF) emitters for organic light-emitting diodes (OLEDs), Beilstein J. Org. Chem. 14 (2018) 282–308, https://doi.org/10.3762/bjoc.14.18.
[16] Y. Li, J.-Y. Liu, Y.-D. Zhao, Y.-C. Cao, Recent advancements of high efficient donor-acceptor type blue small molecule applied for OLEDs, Mater. Today 20 (2017) 258–266, https://doi.org/10.1016/j.mattod.2016.12.003.
[17] M. Zhu, C. Yang, Blue fluorescent emitters: design tactics and applications in organic light-emitting diodes, Chem. Soc. Rev. 42 (2013) 4963–4976, https://doi.org/10.1039/C3CS35440G.
[18] R. Pode, Organic light emitting diode devices: An energy efficient solid state lighting for applications, Renew. Sust. Energ. Rev. 133 (2020), 110043, https://doi.org/10.1016/j.rser.2020.110043.
[19] C. Bizzarri, E. Spuling, D.M. Knoll, D. Volz, S. Bräse, Sustainable metal complexes for organic light-emitting diodes (OLEDs), Coord. Chem. Rev. 373 (2018) 49–82, https://doi.org/10.1016/j.ccr.2017.09.011.
[20] D. Volz, Review of organic light-emitting diodes with thermally activated delayed fluorescence emitters for energy-efficient sustainable light sources and displays, J. Photonics Energy 6 (2016), 020901, https://doi.org/10.1117/1.JPE.6.020901.
[21] C. Wegeberg, O.S. Wenger, Luminescent first-row transition metal complexes, JACS Au 1 (2021) 1860–1876, https://doi.org/10.1021/jacsau.1c00353.
[22] P. Tao, S.-J. Liu, W.-Y. Wong, Phosphorescent manganese(II) complexes and their emerging applications, Adv. Opt. Mater. 8 (2020) 2000985, https://doi.org/10.1002/adom.202000985.
[23] Y. Qin, P. She, X. Huang, W. Huang, Q. Zhao, Luminescent manganese(II) complexes: Synthesis, properties and optoelectronic applications, Coord. Chem. Rev. 416 (2020), 213331, https://doi.org/10.1016/j.ccr.2020.213331.
[24] A.V. Artem'ev, M.P. Davydova, A.S. Berezin, V.K. Brel, V.P. Morgalyuk, I. Y. Bagryanskaya, D.G. Samsonenko, Luminescence of the Mn^{2+} ion in non-O_h and T_d coordination environments: the missing case of square pyramid, Dalton Trans. 48 (2019) 16448–16456, https://doi.org/10.1039/C9DT03283E.
[25] Y. Wu, X. Zhang, L.-J. Xu, M. Yang, Z.-N. Chen, Luminescent vapochromism due to a change of the ligand field in a one-dimensional manganese(II) coordination polymer, Inorg. Chem. 57 (2018) 9175–9181, https://doi.org/10.1021/acs.inorgchem.8b01205.
[26] Y. Wu, X. Zhang, Y.-Q. Zhang, M. Yang, Z.-N. Chen, Achievement of ligand-field induced thermochromic luminescence via two-step single-crystal to single-crystal transformations, Chem. Commun. 54 (2018) 13961–13964, https://doi.org/10.1039/C8CC08665F.
[27] Y.-Y. Tang, Z.-X. Wang, P.-F. Li, Y.-M. You, A. Stroppa, R.-G. Xiong, Brilliant triboluminescence in a potential organic–inorganic hybrid ferroelectric: $(Ph_3PO)_2MnBr_2$, Inorg. Chem. Front. 4 (2017) 154–159, https://doi.org/10.1039/C6QI00148C.
[28] X. Huang, Y. Qin, P. She, H. Meng, S. Liu, Q. Zhao, Functionalized triphenylphosphine oxide-based manganese(II) complexes for luminescent printing, Dalton Trans. 50 (2021) 8831–8836, https://doi.org/10.1039/D1DT00914A.
[29] J. Chen, Q. Zhang, F.-K. Zheng, Z.-F. Liu, S.-H. Wang, A.-Q. Wu, G.-C. Guo, Intense photo- and tribo-luminescence of three tetrahedral manganese(II) dihalides with chelating bidentate phosphine oxide ligand, Dalton Trans. 44 (2015) 3289–3294, https://doi.org/10.1039/C4DT03694H.
[30] A.S. Berezin, M.P. Davydova, I.Y. Bagryanskaya, O.I. Artyushin, V.K. Brel, A. V. Artem'ev, A red-emitting Mn(II)-based coordination polymer build on 1,2,4,5-tetrakis(diphenylphosphinyl)benzene, Inorg. Chem. Commun. 107 (2019), 107473, https://doi.org/10.1016/j.inoche.2019.107473.
[31] A.V. Artem'ev, M.P. Davydova, A.S. Berezin, T.S. Sukhikh, D.G. Samsonenko, Photo- and triboluminescent robust 1D polymers made of Mn(II) halides and meta-carborane based bis(phosphine oxide), Inorg. Chem. Front. 8 (2021) 2261–2270, https://doi.org/10.1039/D1QI00036E.
[32] A.V. Artem'ev, M.P. Davydova, M.I. Rakhmanova, I.Y. Bagryanskaya, D. P. Pishchur, A family of Mn(II) complexes exhibiting strong photo- and triboluminescence as well as polymorphic luminescence, Inorg. Chem. Front. 8 (2021) 3767–3774, https://doi.org/10.1039/D1QI00556A.
[33] Y. Qin, P. Tao, L. Gao, P. She, S. Liu, X. Li, F. Li, H. Wang, Q. Zhao, Y. Miao, W. Huang, Designing Highly Efficient Phosphorescent Neutral Tetrahedral Manganese(II) Complexes for Organic Light-Emitting Diodes, Adv. Optical Mater. 7 (2019) 1801160, https://doi.org/10.1002/adom.201801160.
[34] M. Bortoluzzi, J. Castro, E. Trave, D. Dallan, S. Favaretto, Orange-emitting manganese(II) complexes with chelating phosphine oxides, Inorg. Chem. Commun. 90 (2018) 105–107, https://doi.org/10.1016/j.inoche.2018.02.018.
[35] H. Meng, W. Zhu, F. Li, X. Huang, Y. Qin, S. Liu, Y. Yang, W. Huang, Q. Zhao, Highly emissive and stable five-coordinated manganese(II) complex for X-ray imaging, Laser Photonics Rev. 15 (2021) 2100309, https://doi.org/10.1002/lpor.202100309.
[36] M. Bortoluzzi, J. Castro, F. Enrichi, A. Vomiero, M. Busato, W. Huang, Green-emitting manganese (II) complexes with phosphoramide and phenylphosphonic diamide ligands, Inorg. Chem. Commun. 92 (2018) 145–150, https://doi.org/10.1016/j.inoche.2018.04.023.
[37] M. Bortoluzzi, J. Castro, Dibromomanganese(II) complexes with hexamethylphosphoramide and phenylphosphonic bis(diamide) ligands, J. Coord. Chem. 72 (2019) 309–327, https://doi.org/10.1080/00958972.2018.1560430.
[38] M. Bortoluzzi, J. Castro, A. Gobbo, V. Ferraro, L. Pietrobon, S. Antoniutti, Tetrahedral photoluminescent manganese(II) halide complexes with 1,3-dimethyl-2-phenyl-1,3-diazaphospholidine-2-oxide as a ligand, New J. Chem. 44 (2020) 571–579, https://doi.org/10.1039/C9NJ05083C.
[39] M. Bortoluzzi, J. Castro, A. Gobbo, V. Ferraro, L. Pietrobon, Light harvesting indolyl-substituted phosphoramide ligand for the enhancement of Mn(II) luminescence, Dalton Trans. 49 (2020) 7525–7534, https://doi.org/10.1039/D0DT01659D.
[40] M. Bortoluzzi, J. Castro, A. Di Vera, A. Palù, V. Ferraro, Manganese(II) bromo- and iodo-complexes with phosphoramidate and phosphonate ligands: synthesis, characterization and photoluminescence, New J. Chem. 45 (2021) 12871–12878, https://doi.org/10.1039/D1NJ02053F.
[41] F. Dumur, Zinc complexes in OLEDs: An overview, Synth. Met. 195 (2014) 241–1151, https://doi.org/10.1016/j.synthmet.2014.06.018.
[42] L. Li, Z.-P. Wang, G.-R. Tian, X.-Y. Song, S.-X. Sun, Growth and properties of dichloro bis(triphenylphosphine oxide) zinc(II), a novel nonlinear optical crystal, J. Cryst. Growth 310 (2008) 1202–1205, https://doi.org/10.1016/j.jcrysgro.2007.12.058.
[43] V. Ferraro, F. Baggio, J. Castro, M. Bortoluzzi, Green Phosphorescent Zn(II) Halide Complexes with *N,N,N',N'*-tetramethyl-P-indol-1-ylphosphonic Diamide as Ligand, Eur. J. Inorg. Chem. (2022), https://doi.org/10.1002/ejic.202200119.
[44] M. Bortoluzzi, V. Ferraro, J. Castro, Synthesis and photoluminescence of manganese(II) naphtylphosphonic diamide complexes, Dalton Trans. 50 (2021) 3132–3136, https://doi.org/10.1039/D1DT00123J.
[45] M. Bortoluzzi, J. Castro, V. Ferraro, Dual emission from Mn(II) complexes with carbazolyl-substituted phosphoramides, Inorg. Chim. Acta 536 (2022), 120896, https://doi.org/10.1016/j.ica.2022.120896.
[46] A.S. Berezin, D.G. Samsonenko, V.K. Brelc, A.V. Artem'ev, "Two-in-one" organic–inorganic hybrid Mn^{II} complexes exhibiting dual-emissive phosphorescence, Dalton Trans. 47 (2018) 7306–7315, https://doi.org/10.1039/C8DT01041B.
[47] M.P. Davydova, I.A. Bauer, V.K. Brel, M.I. Rakhmanova, I.Y. Bagryanskaya, A. V. Artem'ev, Manganese(II),, Thiocyanate complexes with Bis(phosphine Oxide) ligands: synthesis and excitation wavelength-dependent multicolor luminescence, Eur. J. Inorg. Chem. (2020) 695–703, https://doi.org/10.1002/ejic.201901213.
[48] Z. Bai, L. Song, Y. Hu, R.K.K. Yuen, Preparation, flame retardancy, and thermal degradation of unsaturated polyester resin modified with a novel phosphorus containing acrylate, Ind. Eng. Chem. Res. 52 (2013) 12855–12864, https://doi.org/10.1021/ie401662x.
[49] Y. Lin, S. Jiang, Z. Gui, G. Li, X. Shi, G. Chen, X. Peng, Synthesis of a novel highly effective flame retardant containing multivalent phosphorus and its application in unsaturated polyester resins, RSC Adv. 6 (2016) 86632–86639, https://doi.org/10.1039/C6RA19798A.
[50] H. Wang, S. Wang, X. Du, H. Wang, X. Cheng, Z. Du, Synthesis of a novel flame retardant based on DOPO derivatives and its application in waterborne polyurethane, RSC Adv. 9 (2019) 7411–7419, https://doi.org/10.1039/C8RA09838G.

[51] Y.K. Chen, Q.X. Lu, G. Zhong, H.G. Zhang, M.F. Chen, C.P. Liu, DOPO-based curing flame retardant of epoxy composite material for char formation and intumescent flame retardance, J. Appl. Polym. Sci. 138 (2021) 49918, https://doi.org/10.1002/app.49918.
[52] K.A. Salmeia, S. Gaan, An overview of some recent advances in DOPO-derivatives: Chemistry and flame retardant applications, Polym. Degrad. Stab. 113 (2015) 119–134, https://doi.org/10.1016/j.polymdegradstab.2014.12.014.
[53] J. Vasiljević, M. Čolović, N. Čelan Korošin, M. Šobak, Ž. Štirn, I. Jerman, Effect of Different Flame-Retardant Bridged DOPO Derivatives on Properties of in Situ Produced Fiber-Forming Polyamide 6, Polymers 12 (2020) 657, https://doi.org/10.3390/polym12030657.
[54] T. Stelzig, L. Bommer, S. Gaan, A. Buczko, DOPO-Based Hybrid Flame Retardants (2017) US20170081590A1.
[55] S. Gaan, M. Neisius, P. Mercoli, S. Liang, H. Mispreuve, R. Näscher, Novel phosphonamidates-synthesis and flame retardant application (2013) WO2013020696A2.
[56] W.L.F. Armarego, C.L.L. Chai, Purification of Laboratory Chemicals, 5th ed., Butterworth-Heinemann, London, 2003.
[57] D.J. Pietrzyk, C.W. Frank, Analytical Chemistry, 2nd ed., Academic Press, New York, 2012.
[58] G.A. Bain, J.F. Berry, Diamagnetic corrections and Pascal's constants, J. Chem. Educ. 85 (2008) 532–536, https://doi.org/10.1021/ed085p532.
[59] APEX3, SMART, SAINT, Bruker AXS Inc., Madison, Wisconsin, USA, 2015.
[60] P. McArdle, Oscail, a program package for small-molecule single-crystal crystallography with crystal morphology prediction and molecular modelling, J. Appl. Crystallogr. 50 (2017) 320–326, https://doi.org/10.1107/S1600576716018446.
[61] G.M. Sheldrick, SHELXT – Integrated space-group and crystal-structure determination, Acta Crystallogr, Sect. A: Found. Crystallogr. 71 (2015) 3–8, https://doi.org/10.1107/S2053273314026370.
[62] G.M. Sheldrick, Crystal structure refinement with SHELXL, Acta Crystallogr, Sect. C: Struct. Chem. 71 (2015) 3–8, https://doi.org/10.1107/S2053229614024218.
[63] A.L. Spek, checkCIF validation ALERTS: what they mean and how to respond, Acta Crystallogr. E 76 (2020) 1–11, https://doi.org/10.1107/S2056989019016244.
[64] H.S. Yu, X. He, S.L. Li, D.G. Truhlar, MN15: a Kohn-Sham global-hydrid exchange-correlation density functional with broad accuracy for multi-reference and single-reference systems and noncovalent interactions, Chem. Sci. 7 (2016) 5032–5051, https://doi.org/10.1039/c6sc00705h.
[65] F. Weigend, R. Ahlrichs, Balanced basis sets of split valence, triple zeta valence and quadruple zeta valence quality for H to Rn: Design and assessment of accuracy, Phys. Chem. Chem. Phys. 7 (2005) 3297–3305, https://doi.org/10.1039/B508541A.
[66] M. Cossi, N. Rega, G. Scalmani, V. Barone, Energies, structures, and electronic properties of molecules in solution with the C-PCM solvation model, J. Comput. Chem. 24 (2003) 669–681, https://doi.org/10.1002/jcc.10189.
[67] V. Barone, M. Cossi, Quantum Calculation of Molecular Energies and Energy Gradients in Solution by a Conductor Solvent Model, J. Phys. Chem. A 102 (1998) 1995–2001, https://doi.org/10.1021/jp9716997.
[68] C.J. Cramer, Essentials of Computational Chemistry, 2nd ed., Wiley, Chichester, 2004.
[69] C.A. Ullrich, Time-Dependent Density Functional Theory, Oxford University Press, Oxford, 2012.
[70] M.J. Frisch G.W. Trucks H.B. Schlegel G.E. Scuseria M.A. Robb J.R. Cheeseman G. Scalmani V. Barone G.A. Petersson H. Nakatsuji X. Li M. Caricato A.V. Marenich J. Bloino B.G. Janesko R. Gomperts B. Mennucci H.P. Hratchian J.V. Ortiz A.F. Izmaylov J.L. Sonnenberg D. Williams-Young F. Ding F. Lipparini F. Egidi J. Goings B. Peng A. Petrone T. Henderson D. Ranasinghe V.G. Zakrzewski J. Gao N. Rega G. Zheng W. Liang M. Hada M. Ehara K. Toyota R. Fukuda J. Hasegawa M. Ishida T. Nakajima Y. Honda O. Kitao H. Nakai T. Vreven K. Throssell J.A. Montgomery Jr. J.E. Peralta F. Ogliaro M.J. Bearpark J.J. Heyd E.N. Brothers K.N. Kudin V.N. Staroverov T.A. Keith R. Kobayashi J. Normand K. Raghavachari A.P. Rendell J.C. Burant S.S. Iyengar J. Tomasi M. Cossi J.M. Millam M. Klene C. Adamo R. Cammi J. W. Ochterski R.L. Martin K. Morokuma O. Farkas J.B. Foresman D.J. Fox Gaussian 16, Revision C.01, Gaussian Inc 2016 Wallingford CT.
[71] T. Lu, F. Chen, Multiwfn: A multifunctional wavefunction analyzer, J. Comput. Chem. 33 (2012) 580–592, https://doi.org/10.1002/jcc.22885.
[72] K. Nakamoto, Infrared and Raman Spectra of Inorganic and Coordination Compounds Part B: Applications in Coordination, Organometallic, and Bioinorganic Chemistry, 6th Ed., Wiley, Hoboken, 2009.
[73] S.P. Sinha, T.T. Pakkanen, T.A. Pakkanen, L. Niinistö, Preparation, spectral properties and the crystal structure of the pentacoordinated trichlorobis (hexamethylphosphoramide)-indium(III) complex, Polyhedron 1 (1982) 355–359, https://doi.org/10.1016/S0277-5387(00)80819-0.
[74] D.M.L. Goodgame, F.A. Cotton, Phosphine oxide complexes. Part V. Tetrahedral complexes of manganese(II) containing triphenylphosphine oxide, and triphenylarsine oxide as ligands, J. Chem. Soc. (1961) 3735–3741, https://doi.org/10.1039/jr9610003735.
[75] C.A. Kosky, J.P. Gayda, J.F. Gibson, S.F. Jones, D.J. Williams, Crystal structures of dichlorobis(triphenylphosphine oxide)zinc(II) and dibromobis(triphenylphosphine oxide)zinc(II) and an EPR study of manganese(II) in dibromobis (triphenylphosphine oxide)zinc(II), Inorg. Chem. 21 (1982) 3173–3179, https://doi.org/10.1021/ic00138a051.
[76] L. Yang, D.R. Powell, R.P. Houser, Structural variation in copper(I) complexes with pyridylmethylamide ligands: structural analysis with a new four-coordinate geometry index, τ4, Dalton Trans. (2007) 955–964, https://doi.org/10.1039/b617136b.
[77] A. Okuniewski, D. Rosiak, J. Chojnacki, B. Becker, Coordination polymers and molecular structures among complexes of mercury(II) halides with selected 1-benzoylthioureas, Polyhedron 90 (2015) 47–57, https://doi.org/10.1016/j.poly.2015.01.035.
[78] J. Cirera, E. Ruiz, S. Alvarez, Continuous Shape Measures as a Stereochemical Tool in Organometallic Chemistry, Organometallics 24 (2005) 1556–1562, https://doi.org/10.1021/om049150z.
[79] S. Alvarez, P. Alemany, D. Casanova, J. Cirera, M. Llunell, D. Avnir, Shape maps and polyhedral interconversion paths in transition metal chemistry, Coord. Chem. Rev. 249 (2005) 1693–1708, https://doi.org/10.1016/j.ccr.2005.03.031.
[80] D. Cremer, J.A. Pople, General definition of ring puckering coordinates, J. Am. Chem. Soc. 97 (1975) 1354–1358, https://doi.org/10.1021/ja00839a011.
[81] M. Wrighton, D. Ginley, Excited state decay of tetrahalomanganese(ii) complexes, Chem. Phys. 4 (1974) 295–299, https://doi.org/10.1016/0301-0104(74)80097-2.